Environmental Science & Technology

pubs.acs.org/est

Article

Important Role of Concave Surfaces in Deposition of Colloids under Favorable Conditions as Revealed by Microscale Visualization

Tiantian Li, Chongyang Shen,* William P. Johnson, Huilian Ma, Chao Jin, Chenxi Zhang, Xianxian Chu, Ke Ma, and Baoshan Xing*

Cite This: *Environ. Sci. Technol.* 2022, 56, 4121−4131

Read Online

ACCESS | Metrics & More | Article Recommendations | Supporting Information

ABSTRACT: This study conducted saturated column experiments to systematically investigate deposition of 1 μm positively charged polystyrene latex micro-colloids (representing microplastic particles) on negatively charged rough sand, glass beads, and soil with pore water velocities (PWV) from 4.9×10^{-5} to 8.8×10^{-4} m/s. A critical value of PWV was found below which colloidal attachment efficiency (AE) increased with increasing PWV. The increase in AE with PWV was attributed to enhanced delivery of the colloids and subsequent attachment at concave locations of rough collector surfaces. The AE decreased with further increasing PWV beyond the threshold because the convex sites became unavailable for colloid attachment. By simulating the rough surfaces using the Weierstrass−Mandelbrot equation, the extended Derjaguin−Landau−Verwey−Overbeek (XDLVO) interaction energy calculations and torque analysis revealed that the adhesive torques could be reduced to be comparable or smaller than hydrodynamic torques even under the favorable conditions. Interestingly, scanning electron microscopic experiments showed that blocking occurred at convex sites at all ionic strengths (ISs) (e.g., even when the colloid−colloid interaction was attractive), whereas at concave sites, blocking and ripening (i.e., attached colloids favor subsequent attachment) occurred at low and high ISs, respectively. To our knowledge, our work was the first to show coexistence of blocking and ripening at high ISs due to variation of the collector surface morphology.

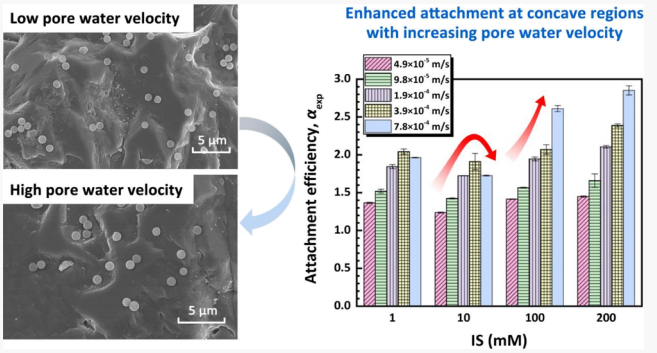

KEYWORDS: *colloids, porous media, deposition, transport, XDLVO interaction*

INTRODUCTION

Investigation of transport of colloids including nanoparticles in porous media has received much attention for several decades due to a variety of environmental concerns.[1−4] For example, microplastic particles have been found to be widely present in subsurface environments such as soil porous media.[5,6] The potential risks of microplastics and microplastic-associated pollutants to groundwater are highly related to their fate and transport behavior in soil. In addition, nanomaterials such as nanoscale zerovalent iron (nZVI) have been shown to have the advantage for wastewater treatment due to their high efficiency for contaminant removal.[7−10] Understanding the transport of nZVI in soil is important for extending the application of nZVI to in situ soil remediation because the efficiency of remediation highly depends on the mobility of the nanomaterials to the contaminant sites.[11,12]

Deposition is one of the primary processes that control transport of colloids in porous media.[13] Colloid deposition is regulated by extended Derjaguin−Landau−Verwey−Overbeek (XDLVO) interaction energies between a colloid and a collector surface, including van der Waals attraction (VDW), electrical double layer (DL) energy, and short-range forces (e.g., hydration and steric repulsion).[14] When the colloid and collector surfaces are oppositely charged, no repulsive interaction energy exists beyond the primary minimum of an interaction energy profile, constructed by a sum of the aforementioned interaction energies as a function of separation distance. Consequently, colloids are favorable to be deposited at the primary minimum due to attractive interaction energies.[15,16]

Existing theoretical calculations can correctly predict the variation of colloid deposition in porous media under the favorable conditions.[4,17,18] For instance, various correlation equations were developed based on well-known colloid filtration theory (CFT), which successfully predicted the variation of the deposition rate with colloid size (e.g., the rate reaches the minimum for colloid sizes around 1 μm).[13,19−21]

Received: October 27, 2021
Revised: March 9, 2022
Accepted: March 10, 2022
Published: March 21, 2022

These correlation equations considered three individual deposition mechanisms (i.e., Brownian diffusion, interception, and gravitational sedimentation) and VDW energy and hydrodynamics. Elimelech,[22] through further including DL energy, theoretically examined the influence of solution ionic strength (IS) on deposition of colloids in porous media under favorable conditions. The deposition was found to increase modestly with decreasing IS due to increase in the range and magnitude of the attractive DL interactions.

The above-mentioned theoretical predictions on the variation of colloid deposition with colloid size and IS have been confirmed by numerous experimental studies.[4,13] However, existing theoretical calculations still cannot exactly estimate the colloid deposition rate under favorable conditions, although the discrepancies are not so significant as those observed under unfavorable conditions.[17] Surface roughness has been identified as a critical factor influencing colloid deposition under unfavorable conditions.[23−25] Recent studies[26−30] showed that surface roughness also played a critical role in regulating colloid deposition under favorable conditions. However, the mechanisms controlling the colloid deposition in the presence of surface roughness under the favorable conditions remain to be elucidated to date. For example, while Chen et al.[31] showed an increased deposition rate with increasing surface roughness, the decrease in or nonmonotonic variation of the deposition rate as a result of increased roughness was also reported.[26−30]

It is worth mentioning that the aforementioned studies commonly used a single roughness parameter such as average roughness (R_a) and root-mean-square (rms) roughness (R_q, the normalized roughness parameters using colloid/collector diameter) to characterize the roughness degree. However, these parameters only represent mean values, which do not provide specific information on the local variation of surface geometry.[4] The influence of local variability of a rough surface profile (e.g., concave and convex geometries) on the deposition of colloids under favorable conditions has not been examined to date. The response of the deposition at different surface geometries to variation of system conditions such as flow and pore water velocity (PWV) is still unclear, which may be responsible for the inconsistent variation of the deposition rate with surface roughness.

This study systematically examined influence of surface roughness on deposition of positively charged polystyrene latex particles (1 μm) in saturated columns packed with negatively charged sand and glass beads. Special attention was paid on direct observation of local deposition of the colloids on rough collector surfaces using scanning electron microscopy (SEM) at different ISs with different PWVs. To interpret the column and SEM observations, rough surfaces were simulated using Weierstrass−Mandelbrot (W-M) and cosinusoidal functions, and the XDLVO interaction energies between the modeled rough surfaces and microparticles were calculated. A Lagrangian colloid trajectory model was adopted to determine the single-collector contact efficiency η_0 through assuming smooth collector surfaces and a perfect sink (PS) boundary condition. The attachment efficiencies were introduced to quantify the influence of the surface roughness or curvature on attachment. The trajectory model was also used to examine the surface roughness effect on colloid deposition without decoupling the attachment from the transport step. The findings in this work have important implications for delivery of positively charged particles (e.g., nZVI) for in situ soil remediation and prediction of fate and transport of toxic colloids (e.g., microplastics) and colloid-associated contaminants in subsurface environments.

MATERIALS AND METHODS

Colloids and Porous Media. White polystyrene latex microspheres (1 μm in diameter) with amine functional groups (Fisher Scientific Inc.) were adopted. The microparticles are hydrophilic and positively charged. The density of the microparticles is 1.055 g/cm^3 according to the manufacturer. The stock colloid suspensions were diluted in NaCl solutions at different solution ISs (1, 10, 100, and 200 mM) to prepare influent suspensions with a concentration of 10 mg/L for column transport experiments. The pH of the influent suspensions was maintained to be 7 using 1 mM $NaHCO_3$. Note that the addition of $NaHCO_3$ was included in calculation of the solution IS.

Both sand and glass beads with sizes ranging from 212 to 425 μm were employed as model collectors with different degrees of surface roughness. The sand and glass beads were purchased from Sinopharm Group Co., Ltd. (Beijing, China) and Huayu Glass Beads Co., Ltd. (Gu'an, Hebei, China), respectively. The method of Elimelech and O'Melia[32] was modified to clean the sand and glass beads. Briefly, the collectors were soaked with 1 M HNO_3 for 6 h and then thoroughly rinsed with deionized (DI) water and dried in an oven at 105 °C. Using Mastersizer 3000 (Malvern Instruments Ltd., Southborough, Massachusetts), the average sizes of sand and glass beads were measured to be 385 and 358 μm, respectively.

Sizes of the colloids at different solution ISs were measured based on the dynamic light scattering technique using Zetasizer Nano ZS (Malvern Instruments Ltd., Southborough, Massachusetts). Zeta potentials of the colloids and collectors were obtained by determining the electrophoretic mobilities using the zetasizer nano ZS (Malvern Instruments Ltd., Southborough, Massachusetts). Similar to Tufenkji and Elimelech[33] and Li et al.,[34] the collectors were sonicated for 20 min in NaCl at a desired IS, and the supernatant was sampled for measurements of zeta potential. Both atomic force microscopy (AFM) (Dimension Icon, Bruker Co., Karlsruhe, Germany) and SEM (S4800, Hitachi Co., Tokyo, Japan) were used to measure the surface roughness morphology of sand and glass beads. Roughness parameters such as R_a and R_q were also determined by AFM that are necessary for rough surface simulations. Measured zeta potentials of colloids and collectors and sizes of the colloids and determined values of R_a and R_q are shown in Tables S1 and S2 of the Supporting Information. The detailed procedure of roughness measurement via AFM can also be referred to in the Supporting Information.

Column Transport Experiments. Transport experiments were conducted using acrylic columns (1.8 cm inner diameter and 9 cm long) with a top and bottom plate. The cleaned sand particles or glass beads were wet-packed to ensure saturation without any layering. The porosities (f) of all packed sand and glass bead beds were consistently maintained to be 0.41 and 0.36, respectively. The porosities of the packed beds were calculated using the expression $f = 1 - m/\rho V$, where ρ is collector density (2.65 and 2.5 g/cm^3 for sand and glass beads, respectively), m is dry mass of a packed bed, and V is column volume.

Column experiments were performed at approach velocities of 2×10^{-5}, 4×10^{-5}, 8×10^{-5}, 1.6×10^{-4}, and 3.2×10^{-4} m/

https://doi.org/10.1021/acs.est.1c07305
Environ. Sci. Technol. 2022, 56, 4121−4131

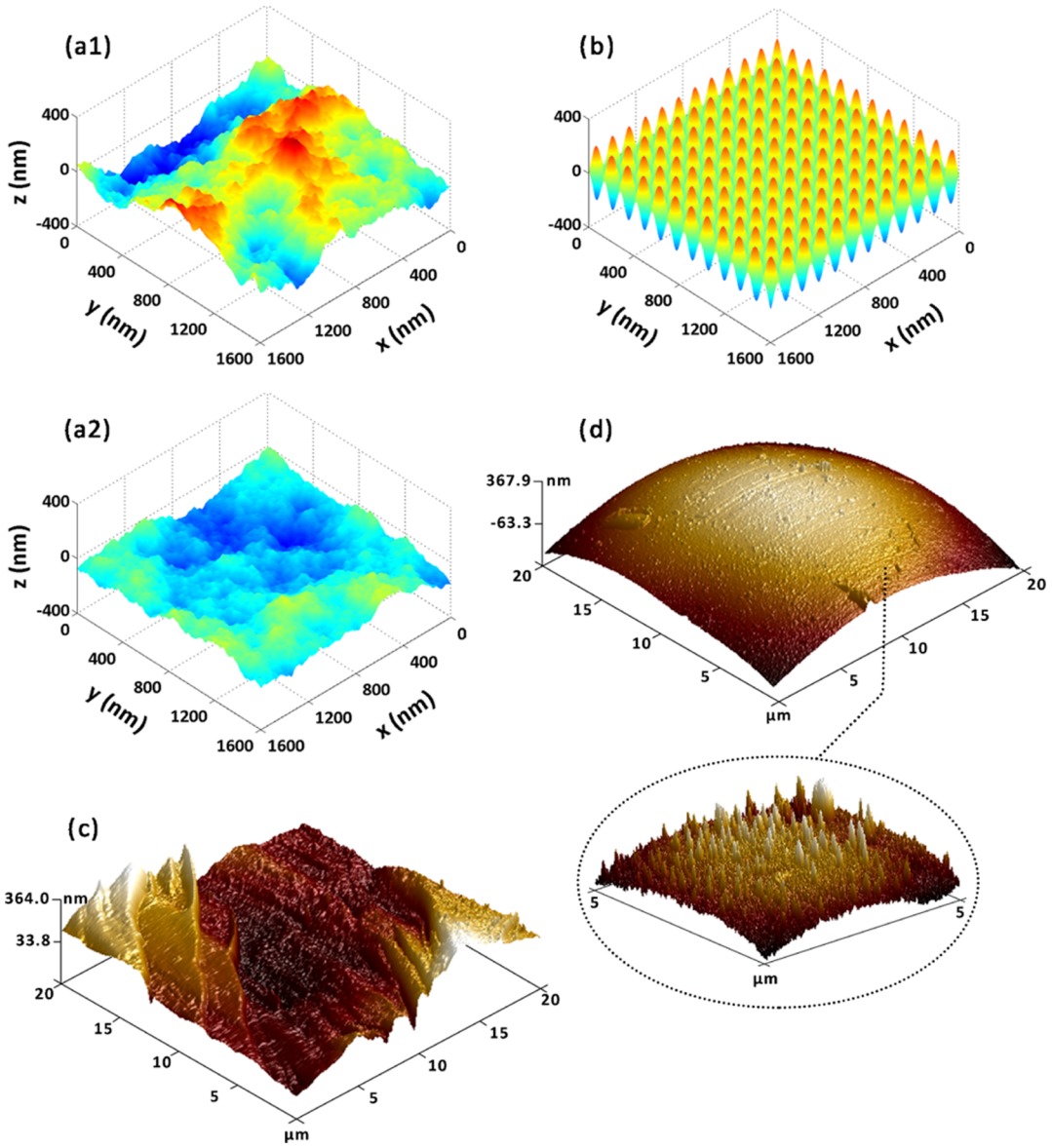

Figure 1. Generated fractal surfaces using the (a) W-M function with G = 0.136 nm and different values of D and $\varphi_{m,n}$ (1, D = 2.268, $\varphi_{m,n}$ is listed in Table S4; 2, D = 2.328, $\varphi_{m,n}$ is listed in Table S5) to simulate the representative surfaces of quartz sand and (b) cosinusoidal function with p = 85 nm and w = 35 nm to simulate the glass bead surface. (c,d) are the real surfaces of quartz sand and glass beads measured by AFM, respectively.

s. The corresponding PWVs in sand columns were 4.9×10^{-5}, 9.8×10^{-5}, 1.9×10^{-4}, 3.9×10^{-4}, and 7.8×10^{-4} m/s. The corresponding PWVs in glass bead columns were 5.6×10^{-5}, 1.1×10^{-4}, 2.2×10^{-4}, 4.4×10^{-4}, and 8.8×10^{-4} m/s. For each experiment, background electrolyte solution was first delivered into the vertical column upward for at least 20 pore volumes (PVs) to standardize chemical conditions of the column system. Then, 5 PVs of the aforementioned colloid suspension at a concentration of 10 mg/L were delivered into the column (phase 1). The unattached colloids in pore water were flushed out of the column by 5 PVs of colloid-free electrolyte solution (phase 2). Finally, 5 PVs of DI water were introduced into the column to examine whether colloids deposited under favorable conditions could be released (phase 3). Note that the colloid suspensions were sonicated for 30 min before introduction into the columns to ensure that the colloids were monodispersed. To avoid sedimentation, the colloid suspensions were stirred during the pumping. Concentrations of colloids in the influent and effluent suspensions were determined via UV−vis spectrophotometry (DU Series 800, Beckman Instruments, Inc., Fullerton, California) at a wavelength of 430 nm (calibration curve shown in Figure S1 of the Supporting Information). After phase 2 or phase 3, the sand and glass beads with attached colloids were sampled and imaged using SEM (S4800, Hitachi Co., Tokyo, Japan) to directly observe the colloidal attachment morphology using the method of Li et al.[35] Note that we have also used the aforementioned procedure to conduct column experiments using real soil. Details about the soil column experiments are shown in the Supporting Information.

The experimental single-collector removal efficiency η_{exp} can be determined using the following expression.[33,36]

$$\eta_{exp} = -\frac{2}{3}\frac{d_c}{(1-f)L}\ln\left(\frac{C}{C_0}\right) \quad (1)$$

https://doi.org/10.1021/acs.est.1c07305
Environ. Sci. Technol. 2022, 56, 4121−4131

where d_c is collector diameter, L is column length, and C and C_0 are effluent and influent colloid concentrations, respectively. Similar to previous studies,[33−35] the value of C/C_0 was obtained by averaging those obtained between 1.8 and 2.0 PV of the breakthrough curves (BTCs) from above-mentioned column experiments. The theoretical single-collector contact efficiency η_0 was calculated using a Lagrangian colloid trajectory model developed by Rasmuson et al.[29,40] by assuming the PS boundary condition and smooth collector surfaces. The Lagrangian colloid trajectory model considers the forces acting on the colloid (including DLVO forces, diffusion, gravity, fluid drag, hydrodynamic retardation, and virtual mass) and predicts the trajectory via Newton's second law of motion. However, as will be shown later in the paper, discrepancies exist between the values of η_{exp} and η or η_0, as have been frequently observed under unfavorable conditions.[4,13,37−39] The discrepancies are mainly because of assuming the PS boundary condition and smooth collector surface. Therefore, the attachment efficiency α was introduced to estimate the surface roughness effect on attachment ($\alpha = \eta/\eta_0$), as frequently done under unfavorable conditions.

In addition to assuming the perfect boundary condition and smooth collector surfaces to decouple attachment from transport, we have also used the Lagrangian colloid trajectory model to simulate the trajectories of colloids from bulk solution to the collector surfaces (without decoupling attachment from transport) to account for the influence of surface roughness and hydrodynamics on colloid deposition. Details about the model have been shown in the Supporting Information, and the model simulations were implemented using the Lagrangian colloid trajectory freeware (Parti-Suite, https://wpjohnsongroup.utah.edu/trajectoryCodes.html) incorporating the hydrodynamic and colloid surface interaction impacts of nanoscale roughness and steric interactions on the surface torque balance (TB).[29,40]

Calculation of XDLVO Interaction Energies and Torque Analysis. The XDLVO interaction energies were determined to interpret the influence of surface roughness on colloid attachment using the surface element integration (SEI) technique.[41,42] The SEM images in Figure S2 of the Supporting Information show that the glass bead surface was smooth, and the sand surface was rough. However, the AFM images (Figure 1) show that the glass bead surfaces exhibited considerable sharp protrusions at the nanoscale (R_a = 69.6 nm). Similar to Li et al.,[34] the cosinusoidal function was used to simulate the glass bead surfaces. The sand surfaces were fractal, which were simulated using the W-M function, as adopted in previous studies.[43−45] Detailed simulation of the fractal surfaces is given in the Supporting Information, and the parameter values used for the simulations are given in Tables S3−S5. Notably, a rough surface contains both convex asperities and concave valleys. As will be shown later in the paper, attachment mechanisms at the two roughness features are different. Therefore, we simulated both convex and concave rough surfaces to separately examine their interactions with colloids.

The SEI technique was adopted to calculate XDLVO interaction energy between a colloid and simulated rough surface (Figure S3). The total XDLVO interaction energy was considered to be a sum of VDW attraction, DL energy, and Born (BR) repulsion (representing short-range repulsion).[34,35,45,46] Both colloid and rough surfaces were discretized into small area elements. The total energy (U) was determined by summing the differential interaction energy between each area element dS on the colloid surface and the corresponding area element dS' on the simulated rough surface. The expressions for quantification of the differential interaction energies are shown in Table S6.

The PS model has been frequently used as the boundary condition for colloid deposition under favorable conditions[13,47] The PS model assumes that colloids near a collector surface experience a very strong attraction that dominates all other applied forces/torques. Therefore, all these colloids will be firmly drawn onto the surface. However, various studies[37,48−52] have indicated that whether a colloid can be deposited under favorable conditions is dependent on the balance between adhesive and hydrodynamic torques (denoted as T_A and T_H, respectively). Therefore, the adhesive and hydrodynamic torques were determined to evaluate the influence of PWV on colloid deposition. The adhesive force was taken as the maximum XDLVO attractive force, and the hydrodynamic force was obtained based on Happel's sphere-in-cell model to describe the flow field. The level arms of adhesive and hydrodynamic torques were dependent on the point of a rough surface around which rolling occurs. Detailed procedures for simulation of sand and glass bead surfaces, TB, and interaction energy calculations are shown in the Supporting Information.

RESULTS AND DISCUSSION

Properties of Colloids and Collectors and Simulation of Rough Surfaces. Table S1 shows measured zeta potentials of the colloids and collectors including sand and glass beads. The values of zeta potentials were negative for sand and glass beads and positive for the colloids under the chemical conditions employed in this study. Therefore, the DL interactions between the colloid and collector surface were attractive, and colloid attachment was considered to be favorable due to absence of repulsive energy barriers. The zeta potential of glass beads was less negative than that of sand. The magnitude of zeta potentials for soil grains was further reduced likely due to the positive-charge heterogeneities. As expected, the magnitude of zeta potential decreased with increasing IS for the colloids and collectors due to DL compression at high ISs. Table S1 also presents the measured sizes of the latex colloids at different solution ISs. The colloid sizes were comparable at ISs of 1, 10, and 100 mM (1270.67, 1304.33, and 1351 nm, respectively) whereas evidently increased at 200 mM (1598.33 nm) due to colloidal aggregation.

Based on the measured surface roughness by AFM examinations in Table S2, the sand and glass bead surfaces were simulated using the W-M and cosinusoidal functions, respectively (see Figure 1). The fractal roughness (G) and fractal dimension (D) of the W-M function are the primary parameters that control the geometry of a fractal surface. Details about the W-M function and the meanings of G and D have been shown in the Supporting Information. In this work, we fixed the value of G to be 0.136 nm, as adopted in previous studies.[45,53] The values of G were adjusted so that the statistical roughness parameters of the simulated surface (R_a and R_q) were exactly matched with those measured from AFM examinations (Tables S2 and S3). For the cosinusoidal surfaces, both the amplitudes (p) and frequencies (w) were adjusted. The W-M function simulated typical concave and convex locations of fractal rough sand surfaces, and the cosinusoidal functions depicted the glass bead surfaces with

https://doi.org/10.1021/acs.est.1c07305
Environ. Sci. Technol. 2022, 56, 4121−4131

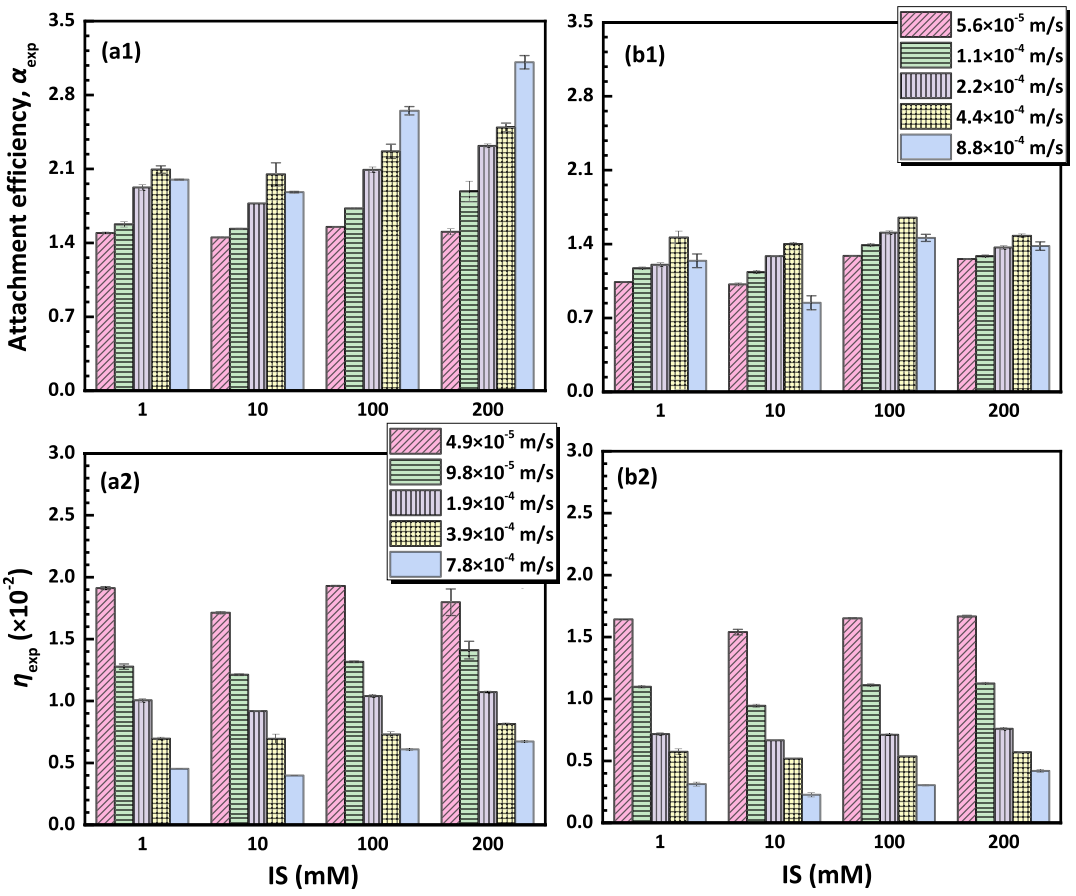

Figure 2. Calculated (1) experimental attachment efficiency α_{exp} and (2) experimental single-collector removal efficiency η_{exp} of the colloids as a function of PWV in (a) quartz sand or (b) glass beads at different ISs. Error bars represent standard deviation from triplicates.

sharp nanoscale protrusions. As shown in Figure 1, the simulated fractal and cosinusoidal surfaces were visually similar to those measured by AFM examinations. However, it should be noted that the actual morphology of the rough surfaces cannot exactly resemble due to randomness of the roughness.[54] The simulated fractal and cosinusoidal surfaces are used for the interaction energy and TB calculations later in the paper.

Attachment Efficiencies. Figures S4 and S5 show BTCs (i.e., plotting the value of C/C_0 as a function of PV) for the positively charged colloids in sand and glass beads, respectively. In phase 1, the colloids were attached at different ISs with different PWVs. At a given solution IS, the deposition or the calculated value of η_{exp} (Figure 2) decreased with increasing PWV. Particularly, almost complete deposition ($C/C_0 \approx 0$) occurred in sand at the lowest PWV (4.9×10^{-5} m/s). This is because increase in PWV decreases single-collector contact efficiency (i.e., the rate at which colloids strike a collector divided by the rate at which colloids flow toward the collector, see Figure S6) due to increase in colloid transport with convective flow (see the calculated value of η_0).

The deposition includes transport from bulk solution to the vicinity of a collector surface and attachment.[13] To exclusively reveal the influence of PWV on the attachment, the values of attachment efficiency α_{exp} were calculated using the method shown previously. A nonmonotonic variation of α_{exp} with PWV was observed (see Figure 2). Specifically, the value of α_{exp} increased with increasing PWV from 4.9×10^{-5} to 3.9×10^{-4} m/s for sand and then decreased with further increasing the PWV in sand at IS $\leq$ 10 mM and in glass beads (see Figure 2). Our results are in contrast to the theoretical predictions of Elimelech and Song[55] that the value of theoretical attachment efficiency ($\alpha_* = \eta/\eta_0$) monotonically increased with increase in PWV. They attributed it to the reason that more colloids can transport from bulk solution to the region where attractive double-layer interactions are important at higher PWVs. In addition, Elimelech and Song[55] theoretically predicted that the increase in attachment efficiency with PWV was more significant at a lower IS because the thickness of attractive DL increased with decreasing IS. Our work, however, showed that the increase in α_{exp} with PWV was similar at all ISs. These discrepancies indicate that in addition to the transport to the attractive DL region, additional mechanisms are involved controlling the deposition of the colloids in the porous media as elucidated in the following.

Figure 3 presents SEM images of deposited colloids on sand surfaces at an IS of 1 and 200 mM with PWVs of 4.9×10^{-5} and 7.8×10^{-4} m/s, respectively. Although the attached colloids were found at both protruding asperities and concave surfaces, the colloids were mainly located at the concave locations, particularly at the high PWVs. For example, by using SEM and randomly selecting 10 locations of a sand surface, we found that only 18 and 4% of attached colloids were located at convex surfaces at 200 mM with PWVs of 4.9×10^{-5} and 7.8×10^{-4} m/s, respectively. These results clearly indicate that the surface roughness morphology plays a critical role in the colloid attachment. Indeed, comparison of Figure S4 with Figure S5 showed that the attachment was reduced in columns packed with glass beads due to their smoother surfaces. In

https://doi.org/10.1021/acs.est.1c07305
Environ. Sci. Technol. 2022, 56, 4121−4131

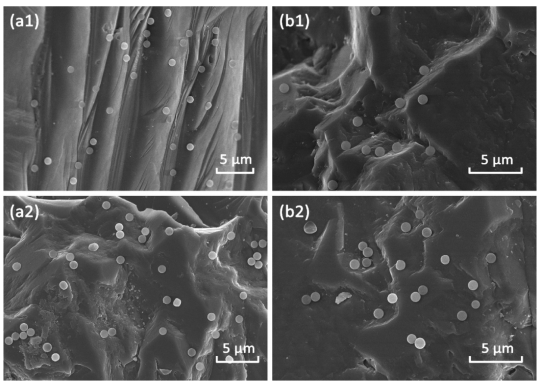

Figure 3. SEM images of quartz sand surfaces taken after deposition under a PWV of (a) 4.9×10^{-5} and (b) 7.8×10^{-4} m/s at different ISs (1, 1 mM; 2, 200 mM).

contrast, if real soil grains were used to pack the columns, the attachment was significantly increased due to the very rough soil grain surfaces (Figures S2 and S7).

One important reason for the observed unfavorable attachment at convex sites is that the tangential components of PWV are increased with increasing PWV. The hydrodynamic shear and drag torque could be increased to be comparable to or even exceed the adhesive torque that acts on a colloid at convex locations (Figure 4). This is because the adhesive forces/torques were significantly reduced at the convex locations compared to those at concave sites due to reduction of the primary minimum depth and accordingly the adhesive forces/torques by the nanoscale protruding heterogeneities (Figure S8 and Table S7). Increase in the PWV also increases the hydrodynamic slip length above convex asperities, resulting in less colloids delivered to these sites.[27,29] Moreover, the values of η_0 were reduced due to the presence of protruding asperities, meaning less colloids delivered to these convex sites (Figure S9). Therefore, the value of α_{exp} decreased with increasing PWV from 3.9×10^{-4} to 7.8×10^{-4} m/s in sand at IS $\leq$ 10 mM and in glass beads, and the attached colloids were mainly distributed at concave locations at the highest PWV. The unfavorable deposition at the convex asperities was further confirmed by the simulations using the Lagrangian colloid trajectory model as shown in Figure 5. Specifically, the nanoscale protruding asperities on collector surfaces can greatly reduce the value of η by reducing colloid−collector attraction and increasing hydrodynamics slip length.

Increase in the PWV (and accordingly its radial components) may increase delivery of the colloids into the concave locations and subsequent attachment because of the increased viscous resistance and stagnant fluid at the concave sites.[56] In addition, the colloids on protruding asperities may roll into the concave regions by hydrodynamic shear. This provides a plausible explanation for the observed increase in α_{exp} with increasing PWV from 4.9×10^{-5} to 3.9×10^{-4} m/s. Note that a monotonic increase in α_{exp} with PWV was observed in sand and soil porous media at IS $\geq$ 100 mM (see Figures 2 and S10). This is because attachment at concave surfaces was the main retention mechanism at these rough sand and soil grain surfaces where considerable large concave locations were accessible to colloid attachment, as observed by the SEM examinations in Figure 3. The dominance of attachment by the concave surface morphology caused the

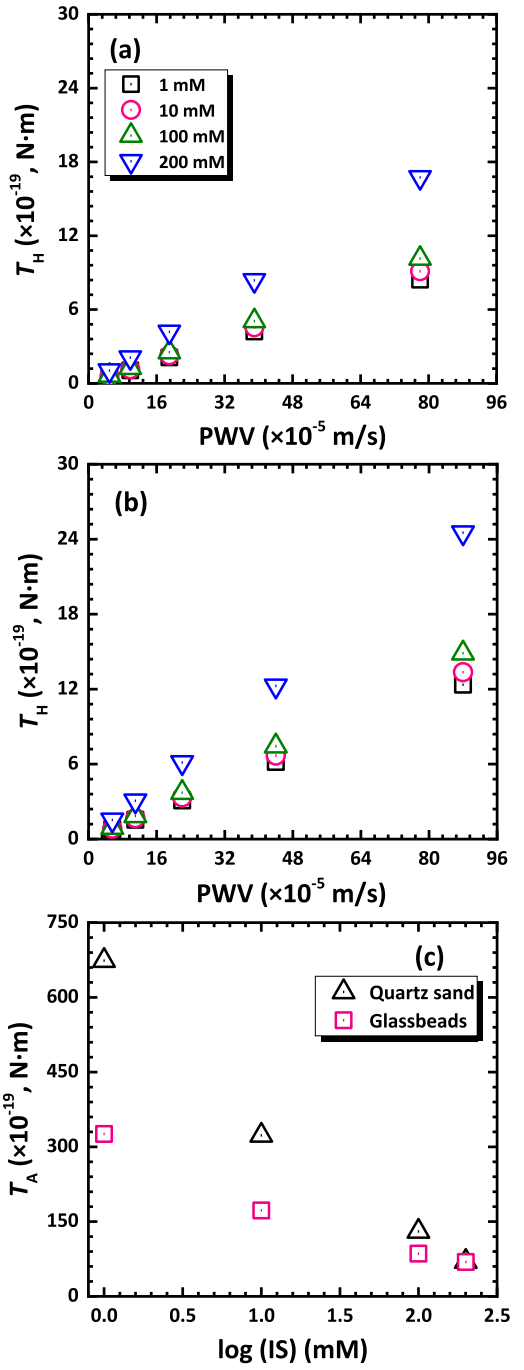

Figure 4. Calculated hydrodynamic torques T_H between a colloid and (a) quartz sand or (b) glass beads as a function of PWV at different ISs. (c) Calculated adhesive torques T_A between a colloid and quartz sand or glass beads as a function of IS.

insensitive variation of α_{exp} with solution IS or the DL thickness.

It is worth mentioning that the primary minimum depth and the adhesive force were shown to increase for a colloid interacting with a concave surface compared to a flat surface in previous studies.[4,29,57] However, these studies modeled concave surfaces consisting of multiple regular smooth surfaces (e.g., two intercepting planar surfaces, between two surfaces of spheres or hemispheres leaning on each other). Our results showed that the primary minimum depth and the adhesive force were significantly reduced at the concave surface when

https://doi.org/10.1021/acs.est.1c07305
Environ. Sci. Technol. 2022, 56, 4121−4131

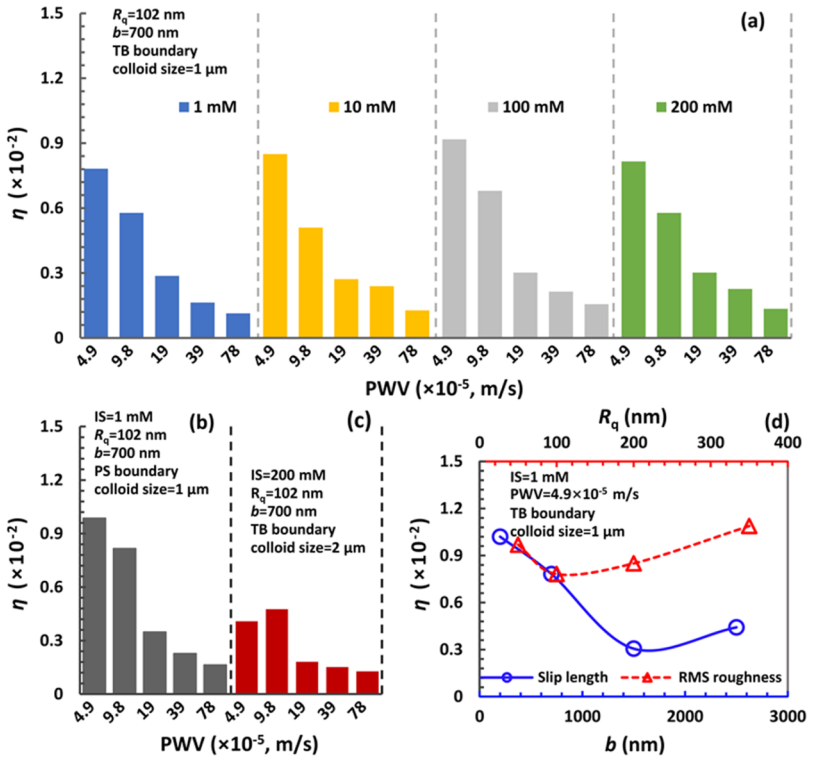

Figure 5. Simulated single-collector efficiency η of the colloids in quartz sand using a Lagrangian colloid trajectory model. (a) Simulated η under a TB boundary condition of 1 μm colloids as a function of PWV (IS = 1, 10, 100, and 200 mM). The collector rms roughness R_q and slip length b were set to 102 and 700 nm, respectively. (b) Simulated η under a PS boundary condition of 1 μm colloids as a function of PWV (IS = 1 mM). The collector R_q and b were set to 102 and 700 nm, respectively. (c) Simulated η under a TB boundary condition of 2 μm colloids as a function of PWV (IS = 200 mM). The collector R_q and b were set to 102 and 700 nm, respectively. (d) Simulated η under a TB boundary condition of 1 μm colloids as a function of b (R_q = 102 nm) or R_q (b = 700 nm) under a PWV of 4.9×10^{-5} m/s and IS of the 1 mM condition.

the fractal of roughness was considered (Table S7). This is because nanoscale protruding asperities exist at the concave locations for fractal surfaces which significantly decrease interaction energies. Therefore, the stable attachment at concave locations may be mainly due to the reduced hydrodynamic shear and drag torque at these regions.

It should be noted that we used a nonretarded expression[58] to calculate VDW energy and assumed a constant surface potential boundary condition[59] to determine DL interaction energy. The primary minimum depth and adhesive force will be decreased if the retarded expression and linear superposition approximation approach are used to calculate the VDW and DL energies, respectively, as adopted in the literature.[60−63] In addition, we adopted a value of 0.158 nm as the minimum separation distance to determine the BR repulsion. The primary minimum depth and adhesive force will be further reduced if a larger value of the shortest separation distance is used (e.g., 1 nm in Li et al.[60−63]). Therefore, the reduction of hydrodynamic shear and drag torque at concave regions may play a more significant role in the stable attachment of colloids at these locations. Although the zeta potentials of sand grains were slightly more negative compared to glass beads which caused deeper primary minima, the insensitive variation of α_{exp} with IS (or zeta potential change) illustrates the relative insignificant contribution of zeta potential to colloid attachment, similar to the observation of Elimelech et al.[64] Note that our work and Elimelech et al's.[64] were conducted under favorable conditions or when the surface heterogeneity was significant. The zeta potential could play a significant role in colloid deposition under unfavorable conditions or when the surface heterogeneity was insignificant as revealed by machine learning examinations.[65−67]

Blocking and Ripening. Figure S4 shows rise and decline of C/C_0 at the plateau of BTCs for sand columns at IS $\leq$ 10 mM and IS $\geq$ 100 mM at high PWVs, respectively. The rise and decline of C/C_0 were interpreted as blocking and ripening, respectively, in the literature.[68−70] Specifically, the colloids attached on collector surfaces influence attachment of subsequently approaching colloids in their vicinity due to geometrical volume excluding the effect and interactions between the attached and approaching colloids.[71] The blocking and ripening mean that attached colloids inhibit and facilitate attachment of the approaching colloids when the colloid−colloid interactions are repulsive and attractive, respectively. The blocking causes attached colloids to be singly and sparsely distributed on collector surfaces (due to side and vertical repulsions between colloids), whereas dense and multilayer deposition can occur due to ripening.

Figure S11 and Table S8 show that repulsive energy barriers exist between colloids at IS $\leq$ 10 mM, whereas the colloid−colloid interaction became attractive at IS $\geq$ 100 mM. The repulsive energies around the attached colloids excluded subsequent attachment around these colloids at the low ISs. Indeed, the SEM images in Figure 3 show that the attached colloids were singly and sparsely distributed at convex sites of rough sand surfaces at 1 mM. Although the attached colloids were more densely distributed at concave locations, significant separation distances (at microscale) still existed between attached colloids. The interaction energy between colloids became insignificant when their separation distances were at

https://doi.org/10.1021/acs.est.1c07305
Environ. Sci. Technol. 2022, 56, 4121−4131

micrometer (Figure S11). In contrast, the attached colloids leaned on each other at concave surfaces at 200 mM when repulsive energy barriers between the colloids disappeared (see Figures 3 and S12).

It is interesting to note that all attached colloids were still singly distributed at convex sites at the highest IS (i.e., individual and sparse deposition, see Figure 3), demonstrating that blocking occurred at these locations even if the colloid−colloid interaction was attractive. It is even more difficult for colloids to be deposited atop the colloids attached at convex locations than directly at the convex locations because the hydrodynamic shear and drag force acting on a colloid are larger in the former case. At the area downgradient of protruding asperities and attached colloids on collector surfaces, Ko and Elimelech[72] demonstrated that a shadow region is created, and this region is not accessible for colloid attachment at high PWVs for large colloids. Colloids that were intercepted with the protruding asperities could roll into the concave regions along the down-gradient side of protrusions due to the nested ring vortices at the concave region. Similarly, at the region up gradient of protruding asperities and attached colloids on collector surfaces (i.e., concave area), colloids can also be driven by the fluid vortices into the vertex of the concave location.[73−77] These reasons may explain the observation of colloids singly distributed at convex sites whereas densely located at concave sites (e.g., nearly saturated layer or multilayer deposition, see Figures 3, 6, and S12). Our

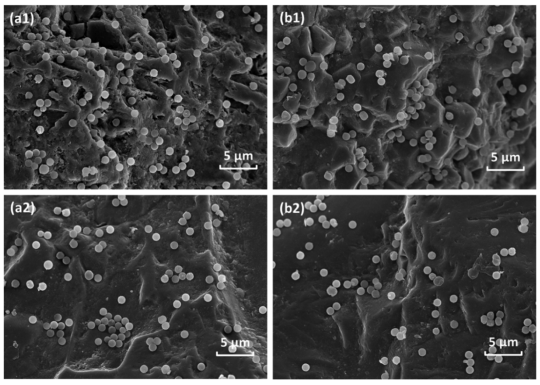

Figure 6. Typical SEM images for soil sand surfaces taken after (1) phase 2 and (2) phase 3 under a PWV of (a) 4.9×10^{-5} and (b) 7.8×10^{-4} m/s at 200 mM. 20 PVs of the colloid influent suspension (50 mg/L) were introduced in phase 1.

experimental observations are in contrast to the theoretical prediction by Kemps and Bhattachharjee[77] that colloids were favorably deposited on protruding asperities in clusters under favorable conditions. It should be mentioned that the densely located colloids at concave locations were not aggregates which showed different morphologies by the SEM examinations (data not shown). In addition, the simulations using the Lagrangian colloid trajectory model illustrated that larger microparticles or colloidal aggregates had lower values of η (Figure 5, panel c).

Detachment. Previous studies[4,29,78] showed that reduction of solution IS can cause detachment of colloids deposited under unfavorable conditions because colloids attached at secondary minima or attached at nanoscale protruding asperities via primary minimum association can be released at low IS due to reduction of depths of primary and secondary minima and expansion of the zone of colloid−surface interaction. Figure S4 shows no detachment of colloids deposited at IS $\leq$ 10 mM under favorable conditions with introduction of DI water to reduce IS in phase 3. This is expected because the attractive interaction between a colloid and collector surface under favorable conditions is larger at a lower IS (Table S7). However, a minor amount of colloids were released in phase 3 when the colloids were initially deposited at IS $\geq$ 100 mM. As mentioned previously, colloids can be deposited at close separation distances at high solution IS. Colloids may be detached when they experience repulsions from nearby colloids exceeding the attractions from collector surfaces at low ISs. Such detachments may become very significant when the concentration of attached colloids is high. Indeed, Figure S7 shows that considerable colloids were released from soil porous media upon reduction of solution IS by increasing injection of PVs of the colloid suspension and colloid concentration. The SEM images of Figure 6 shows that multilayer attachment was even formed, and the retained colloids atop were readily detached at low ISs due to the repulsion from the underlying colloids. Therefore, even positively charged colloids can have great mobility through continuous capture and release when they are at high concentrations in the subsurface environments. Such continuous capture and release of positively charged colloids with high mobility at high input colloid concentrations in porous media of negatively charged collectors have been visually observed.[2] Note that the SEM images of Figure 6 also confirmed that the attachment at concave locations was the main retention mechanism that governed transport of the colloids in the soil porous media, as mentioned previously. In addition to using the high input colloid concentration, Figure S13 shows that if the 50 nm positively charged hematite nanoparticles were initially delivered into the sand columns to mask the attachment sites, the subsequent attachment and detachment of latex colloids were significantly inhibited and enhanced, respectively. It is worthwhile mentioning that Figure S4 shows small tails existing in phase 2 at IS $\leq$ 10 mM, reflecting that a minor amount of colloids were associated with attached colloids on collector surfaces at secondary minima in phase 1 and spontaneously detached in phase 2.

Implications. Nanomaterials such as positively charged nZVI have been shown to be very efficient for removal of a variety of organic and inorganic pollutants from water and wastewater. The application of nanomaterials for in situ groundwater remediation, however, faces challenge because the nanomaterials readily attach on soil and sediment grain surfaces and thus hardly reach contaminated sites. Our work has important implications for delivery of the positively charged nanomaterials for in situ groundwater remediation. For example, our results suggest that it is feasible to initially deliver positively charged particles with low cost to mask the attachment sites in soil, followed by injection of nanomaterial suspensions with high concentrations at high solution ISs and finally reduction of solution IS. Such a procedure could significantly enhance the mobility of the nanomaterials in the subsurface environments.

Our work also has implications for development of models for accurate simulation of transport of colloidal particles such as microplastics and colloid-associated contaminants in porous media. We showed that colloids were singly attached at convex sites at all ISs (even if the colloid−colloid interaction is attractive), reflecting that blocking always occurred at these locations. In contrast, blocking and ripening occurred at low

https://doi.org/10.1021/acs.est.1c07305
Environ. Sci. Technol. 2022, 56, 4121−4131

and high ISs at the concave locations, respectively. Our work for the first time visually showed that blocking and ripening coexisted at high solution ISs. Therefore, it is necessary to improve the existing models that only considered blocking or ripening for accurate prediction of fate and transport of colloids in subsurface environments.

■ ASSOCIATED CONTENT

Supporting Information

The Supporting Information is available free of charge at https://pubs.acs.org/doi/10.1021/acs.est.1c07305.

Details of soil column transport experiments, measurement of surface roughness by AFM, simulation of rough sand and glass bead surfaces, calculation of XDLVO interaction energies between a colloid and rough surface, torque analysis, and description of the colloid trajectory model; zeta potentials of colloids and collectors and sizes of colloids, parameter values used for simulation of rough surfaces, statistical roughness parameters of measured and reconstructed rough surfaces, computer-generated random number for fractal convex and concave surfaces, expressions for calculating XDLVO interaction energies, calculated primary-minimum depths for the colloid interacting with the planar or reconstructed rough surface, calculated maximum energy barriers, detachment energy barriers from primary minimum, and secondary-minimum depths and distances for the interaction between two colloids; and calibration curves for colloid concentration determination, SEM images of collectors, schematic illustration of a spherical colloid interacting with a rough surface, BTCs for colloid transport in sand, glass beads, or soil sand, calculated single-collector removal efficiency or experimental attachment efficiency of the colloids as a function of PWV, calculated XDLVO energy profiles for the colloid-rough/planar surface or colloid−colloid, and typical SEM images for sand surfaces taken after colloid deposition for column transport experiments (PDF)

■ AUTHOR INFORMATION

Corresponding Authors

Chongyang Shen − *Department of Soil and Water Sciences, China Agricultural University, Beijing 100193, China;* orcid.org/0000-0002-2517-3472; Phone: +86 1062732959; Email: chongyang.shen@cau.edu.cn; Fax: +86 1062733596

Baoshan Xing − *Stockbridge School of Agriculture, University of Massachusetts, Amherst, Massachusetts 01003, United States;* orcid.org/0000-0003-2028-1295; Phone: (413) 545-5212; Email: bx@umass.edu; Fax: (413) 577-0242

Authors

Tiantian Li − *School of Environmental Engineering, Henan University of Technology, Zhengzhou, Henan 450001, China; Department of Soil and Water Sciences, China Agricultural University, Beijing 100193, China*

William P. Johnson − *Department of Geology and Geophysics, University of Utah, Salt Lake City, Utah 84112, United States;* orcid.org/0000-0003-3126-3877

Huilian Ma − *Department of Geology and Geophysics, University of Utah, Salt Lake City, Utah 84112, United States*

Chao Jin − *School of Environmental Science and Engineering, Sun Yat-sen University, Guangzhou, Guangdong 510006, China;* orcid.org/0000-0001-6590-333X

Chenxi Zhang − *Department of Soil and Water Sciences, China Agricultural University, Beijing 100193, China*

Xianxian Chu − *Department of Soil and Water Sciences, China Agricultural University, Beijing 100193, China*

Ke Ma − *Department of Soil and Water Sciences, China Agricultural University, Beijing 100193, China*

Complete contact information is available at: https://pubs.acs.org/10.1021/acs.est.1c07305

Notes

The authors declare no competing financial interest.

■ ACKNOWLEDGMENTS

We acknowledge the National Natural Science Foundation of China for financial support (41922047, 41671222, and 42107325) and the 2115 Talent Development Program of China Agricultural University (1191-00109011).

■ ABBREVIATIONS

AFM	atomic force microscopy
BR	Born
BTC	breakthrough curves
CFT	colloid filtration theory
DI	deionized
DL	electrical double layer
IS	ionic strength
nZVI	nanoscale zerovalent iron
PV	pore volume
PWV	pore water velocity
rms	root-mean-square
SEI	surface element integration
SEM	scanning electron microscopy
VDW	van der Waals
W-M	Weierstrass−Mandelbrot
XDLVO	extended Derjaguin−Landau−Verwey−Overbeek

■ REFERENCES

(1) Ma, J.; Guo, H.; Lei, M.; Li, Y.; Weng, L.; Chen, Y.; Ma, Y.; Deng, Y.; Feng, X.; Xiu, W. Enhanced transport of ferrihydrite colloid by chain-shaped humic acid colloid in saturated porous media. *Sci. Total Environ.* **2018**, *621*, 1581−1590.

(2) Bizmark, N.; Schneider, J.; Priestley, R. D.; Datta, S. S. Multiscale dynamics of colloidal deposition and erosion in porous media. *Sci. Adv.* **2020**, *6*, No. eabc2530.

(3) Kim, C.; Pennell, K. D.; Fortner, J. D. Delineating the relationship between nanoparticle attachment efficiency and fluid flow velocity. *Environ. Sci. Technol.* **2020**, *54*, 13992−13999.

(4) Shen, C.; Jin, Y.; Zhuang, J.; Li, T.; Xing, B. Role and importance of surface heterogeneities in transport of particles in saturated porous media. *Crit. Rev. Environ. Sci. Technol.* **2020**, *50*, 244−329.

(5) He, L.; Rong, H.; Wu, D.; Li, M.; Wang, C.; Tong, M. Influence of biofilm on the transport and deposition behaviors of nano- and micro-plastic particles in quartz sand. *Water Res.* **2020**, *178*, 115808.

(6) Keller, A. S.; Jimenez-Martinez, J.; Mitrano, D. M. Transport of nano- and microplastic through unsaturated porous media from sewage sludge application. *Environ. Sci. Technol.* **2020**, *54*, 911−920.

(7) Su, Y.; Adeleye, A. S.; Keller, A. A.; Huang, Y.; Dai, C.; Zhou, X.; Zhang, Y. Magnetic sulfide-modified nanoscale zerovalent iron (S-nZVI) for dissolved metal ion removal. *Water Res.* **2015**, *74*, 47−57.

(8) Zou, Y.; Wang, X.; Khan, A.; Wang, P.; Liu, Y.; Alsaedi, A.; Hayat, T.; Wang, X. Environmental remediation and application of

nanoscale zero-valent iron and its composites for the removal of heavy metal ions: A review. *Environ. Sci. Technol.* **2016**, *50*, 7290−7304.
(9) Srirattana, S.; Piaowan, K.; Lowry, G. V.; Phenrat, T. Electromagnetic induction of foam-based nanoscale zerovalent iron (NZVI) particles to thermally enhance non-aqueous phase liquid (NAPL) volatilization in unsaturated porous media: Proof of concept. *Chemosphere* **2017**, *183*, 323−331.
(10) Xu, J.; Cao, Z.; Wang, Y.; Zhang, Y.; Gao, X.; Ahmed, M. B.; Zhang, J.; Yang, Y.; Zhou, J. L.; Lowry, G. V. Distributing sulfidized nanoscale zerovalent iron onto phosphorus-functionalized biochar for enhanced removal of antibiotic florfenicol. *Chem. Eng. J.* **2019**, *359*, 713−722.
(11) Johnson, R. L.; Nurmi, J. T.; O'Brien Johnson, G. S.; Fan, D.; O'Brien Johnson, R. L.; Shi, Z.; Salter-Blanc, A. J.; Tratnyek, P. G.; Lowry, G. V. Field-scale transport and transformation of carboxymethylcellulose-stabilized nano zero-valent iron. *Environ. Sci. Technol.* **2013**, *47*, 1573−1580.
(12) Zhang, T.; Lowry, G. V.; Capiro, N. L.; Chen, J.; Chen, W.; Chen, Y.; Dionysiou, D. D.; Elliott, D. W.; Ghoshal, S.; Hofmann, T.; Hsu-Kim, H.; Hughes, J.; Jiang, C.; Jiang, G.; Jing, C.; Kavanaugh, M.; Li, Q.; Liu, S.; Ma, J.; Pan, B.; Phenrat, T.; Qu, X.; Quan, X.; Saleh, N.; Vikesland, P. J.; Wang, Q.; Westerhoff, P.; Wong, M. S.; Xia, T.; Xing, B.; Yan, B.; Zhang, L.; Zhou, D.; Alvarez, P. J. J. In situ remediation of subsurface contamination: Opportunities and challenges for nanotechnology and advanced materials. *Environ. Sci.: Nano* **2019**, *6*, 1283−1302.
(13) Ryan, J. N.; Elimelech, M. Colloid mobilization and transport in groundwater. *Colloids Surf., A* **1996**, *107*, 1−56.
(14) Bradford, S. A.; Torkzaban, S. Colloid interaction energies for physically and chemically heterogeneous porous media. *Langmuir* **2013**, *29*, 3668−3676.
(15) Shen, C.; Li, B.; Huang, Y.; Jin, Y. Kinetics of coupled primary- and secondary-minimum deposition of colloids under unfavorable chemical conditions. *Environ. Sci. Technol.* **2007**, *41*, 6976−6982.
(16) Li, K.; Ma, H. Deposition dynamics of rod-shaped colloids during transport in porous media under favorable conditions. *Langmuir* **2018**, *34*, 2967−2980.
(17) Molnar, I. L.; Johnson, W. P.; Gerhard, J. I.; Willson, C. S.; O'Carroll, D. M. Predicting colloid transport through saturated porous media: A critical review. *Water Resour. Res.* **2015**, *51*, 6804−6845.
(18) Babakhani, P.; Bridge, J.; Doong, R.-a.; Phenrat, T. Continuum-based models and concepts for the transport of nanoparticles in saturated porous media: A state-of-the-science review. *Adv. Colloid Interface Sci.* **2017**, *246*, 75−104.
(19) Yao, K.-M.; Habibian, M. T.; O'Melia, C. R. Water and waste water filtration: Concepts and applications. *Environ. Sci. Technol.* **1971**, *5*, 1105−1112.
(20) Tufenkji, N.; Elimelech, M. Correlation equation for predicting single-collector efficiency in physicochemical filtration in saturated porous media. *Environ. Sci. Technol.* **2004**, *38*, 529−536.
(21) Nelson, K. E.; Ginn, T. R. New collector efficiency equation for colloid filtration in both natural and engineered flow conditions. *Water Resour. Res.* **2011**, *47*, W05543.
(22) Elimelech, M. Kinetics of capture of colloidal particles in packed beds under attractive double layer interactions. *J. Colloid Interface Sci.* **1991**, *146*, 337−352.
(23) Fischer, C.; Kurganskaya, I.; Schäfer, T.; Lüttge, A. Variability of crystal surface reactivity: What do we know? *Appl. Geochem.* **2014**, *43*, 132−157.
(24) Kananizadeh, N.; Peev, D.; Delon, T.; Schubert, E.; Bartelt-Hunt, S.; Schubert, M.; Zhang, J.; Uhlmann, P.; Lederer, A.; Li, Y. Visualization of label-free titanium dioxide nanoparticle deposition on surfaces with nanoscale roughness. *Environ. Sci.: Nano* **2019**, *6*, 248−260.
(25) Liang, Y.; Zhou, J.; Dong, Y.; Klumpp, E.; Šimůnek, J.; Bradford, S. A. Evidence for the critical role of nanoscale surface roughness on the retention and release of silver nanoparticles in porous media. *Environ. Pollut.* **2020**, *258*, 113803.
(26) Jin, C.; Normani, S. D.; Emelko, M. B. Surface roughness impacts on granular media filtration at favorable deposition conditions: Experiments and modeling. *Environ. Sci. Technol.* **2015**, *49*, 7879−7888.
(27) Jin, C.; Ren, C. L.; Emelko, M. B. Concurrent modeling of hydrodynamics and interaction forces improves particle deposition predictions. *Environ. Sci. Technol.* **2016**, *50*, 4401−4412.
(28) Rasmuson, A.; Pazmino, E.; Assemi, S.; Johnson, W. P. Contribution of nano- to microscale roughness to heterogeneity: Closing the gap between unfavorable and favorable colloid attachment conditions. *Environ. Sci. Technol.* **2017**, *51*, 2151−2160.
(29) Rasmuson, A.; VanNess, K.; Ron, C. A.; Johnson, W. P. Hydrodynamic versus surface interaction impacts of roughness in closing the gap between favorable and unfavorable colloid transport conditions. *Environ. Sci. Technol.* **2019**, *53*, 2450−2459.
(30) Ron, C. A.; VanNess, K.; Rasmuson, A.; Johnson, W. P. How nanoscale surface heterogeneity impacts transport of nano- to microparticles on surfaces under unfavorable attachment conditions. *Environ. Sci.: Nano* **2019**, *6*, 1921.
(31) Chen, G.; Bedi, R. S.; Yan, Y. S.; Walker, S. L. Initial colloid deposition on bare and zeolite-coated stainless steel and aluminum: Influence of surface roughness. *Langmuir* **2010**, *26*, 12605−12613.
(32) Elimelech, M.; O'Melia, C. R. Kinetics of deposition of colloidal particles in porous media. *Environ. Sci. Technol.* **1990**, *24*, 1528−1536.
(33) Tufenkji, N.; Elimelech, M. Breakdown of colloid filtration theory: Role of the secondary energy minimum and surface charge heterogeneities. *Langmuir* **2005**, *21*, 841−852.
(34) Li, T.; Shen, C.; Wu, S.; Jin, C.; Bradford, S. A. Synergies of surface roughness and hydration on colloid detachment in saturated porous media: Column and atomic force microscopy studies. *Water Res.* **2020**, *183*, 116068.
(35) Li, T.; Jin, Y.; Huang, Y.; Li, B.; Shen, C. Observed dependence of colloid detachment on the concentration of initially attached colloids and collector surface heterogeneity in porous media. *Environ. Sci. Technol.* **2017**, *51*, 2811−2820.
(36) Logan, B. E.; Jewett, D. G.; Arnold, R. G.; Bouwer, E. J.; O'Melia, C. R. Clarification of clean-bed filtration models. *J. Environ. Eng.* **1995**, *121*, 869−873.
(37) Shen, C.; Huang, Y.; Li, B.; Jin, Y. Predicting attachment efficiency of colloid deposition under unfavorable attachment conditions. *Water Resour. Res.* **2010**, *46*, W11526.
(38) Morales, V. L.; Sang, W.; Fuka, D. R.; Lion, L. W.; Gao, B.; Steenhuis, T. S. Correlation equation for predicting attachment efficiency (α) of organic matter-colloid complexes in unsaturated porous media. *Environ. Sci. Technol.* **2011**, *45*, 10096−10101.
(39) Saiers, J. E.; Ryan, J. N. Colloid deposition on non-ideal porous media: The influence of collector shape and roughness on the single-collector efficiency. *Geophys. Res. Lett.* **2005**, *32*, L21406.
(40) Johnson, W. P.; Tong, M. Observed and simulated fluid drag effects on colloid deposition in the presence of an energy barrier in an impinging jet system. *Environ. Sci. Technol.* **2006**, *40*, 5015−5021.
(41) Bhattacharjee, S.; Elimelech, M. Surface element integration: A novel technique for evaluation of DLVO interaction between a particle and a flat plate. *J. Colloid Interface Sci.* **1997**, *193*, 273−285.
(42) Duffadar, R. D.; Davis, J. M. Interaction of micrometer-scale particles with nanotextured surfaces in shear flow. *J. Colloid Interface Sci.* **2007**, *308*, 20−29.
(43) Cai, X.; Yang, L.; Wang, Z.; Zhang, M.; Shen, L.; Hong, H.; Lin, H.; Yu, G. Influence of fractal dimension of membrane surface on interfacial interactions related to membrane fouling in a membrane bioreactor. *J. Colloid Interface Sci.* **2017**, *500*, 79−87.
(44) Zhang, M.; Zhou, X.; Shen, L.; Cai, X.; Wang, F.; Chen, J.; Lin, H.; Li, R.; Wu, X.; Liao, B.-Q. Quantitative evaluation of the interfacial interactions between a randomly rough sludge floc and membrane surface in a membrane bioreactor based on fractal geometry. *Bioresour. Technol.* **2017**, *234*, 198−207.
(45) Wang, H.; Zhang, W.; Zeng, S.; Shen, C.; Jin, C.; Huang, Y. Interactions between nanoparticles and fractal surfaces. *Water Res.* **2019**, *151*, 296−309.

https://doi.org/10.1021/acs.est.1c07305
Environ. Sci. Technol. 2022, 56, 4121−4131

(46) Bradford, S. A.; Kim, H.; Shen, C.; Sasidharan, S.; Shang, J. Contributions of nanoscale roughness to anomalous colloid retention and stability behavior. *Langmuir* **2017**, *33*, 10094−10105.
(47) James, S. C.; Chrysikopoulos, C. V. Transport of polydisperse colloid suspensions in a single fracture. *Water Resour. Res.* **1999**, *35*, 707−718.
(48) Bergendahl, J.; Grasso, D. Prediction of colloid detachment in a model porous media: hydrodynamics. *Chem. Eng. Sci.* **2000**, *55*, 1523−1532.
(49) Burdick, G. M.; Berman, N. S.; Beaudoin, S. P. Hydrodynamic particle removal from surfaces. *Thin Solid Films* **2005**, *488*, 116−123.
(50) Torkzaban, S.; Bradford, S. A.; Walker, S. L. Resolving the coupled effects of hydrodynamics and DLVO forces on colloid attachment in porous media. *Langmuir* **2007**, *23*, 9652−9660.
(51) Shen, C.; Bradford, S. A.; Li, T.; Li, B.; Huang, Y. Can nanoscale surface charge heterogeneity really explain colloid detachment from primary minima upon reduction of solution ionic strength? *J. Nanopart. Res.* **2018**, *20*, 165.
(52) VanNess, K.; Rasmuson, A.; Ron, C. A.; Johnson, W. P. A unified force and torque balance for colloid transport: Predicting attachment and mobilization under favorable and unfavorable conditions. *Langmuir* **2019**, *35*, 9061−9070.
(53) Sahoo, P.; Ghosh, N. Finite element contact analysis of fractal surfaces. *J. Phys. D: Appl. Phys.* **2007**, *40*, 4245−4252.
(54) Hoek, E. M. V.; Bhattacharjee, S.; Elimelech, M. Effect of membrane surface roughness on colloid-membrane DLVO interactions. *Langmuir* **2003**, *19*, 4836−4847.
(55) Elimelech, M.; Song, L. Theoretical investigation of colloid separation from dilute aqueous suspensions by oppositely charged granular media. *Sep. Technol.* **1992**, *2*, 2−12.
(56) Myers, T. G. Modeling laminar sheet flow over rough surfaces. *Water Resour. Res.* **2002**, *38*, 1230.
(57) Huang, X.; Bhattacharjee, S.; Hoek, E. M. V. Is surface roughness a "scapegoat" or a primary factor when defining particle-substrate interactions? *Langmuir* **2010**, *26*, 2528−2537.
(58) Hamaker, H. C. The London-van der Waals attraction between spherical particles. *Physica* **1937**, *4*, 1058−1072.
(59) Hogg, R.; Healy, T. W.; Fuerstenau, D. W. Mutual coagulation of colloidal dispersions. *Trans. Faraday Soc.* **1966**, *62*, 1638−1651.
(60) Lee, H.; Segets, D.; Süß, S.; Peukert, W.; Chen, S.-C.; Pui, D. Y. H. Liquid filtration of nanoparticles through track-etched membrane filters under unfavorable and different ionic strength conditions: experiments and modeling. *J. Membr. Sci.* **2017**, *524*, 682−690.
(61) Lee, H.; Kang, S.; Kim, S. C.; Pui, D. Y. H. Modeling transport of colloidal particles through polydisperse fibrous membrane filters under unfavorable chemical and physical conditions. *Powder Technol.* **2019**, *355*, 7−17.
(62) Lee, H.; Kang, S.; Kim, S. C.; Pui, D. Y. H. Deposition and reentrainment of colloidal particles in disordered fibrous filters under chemically and physically unfavorable conditions. *J. Membr. Sci.* **2019**, *582*, 322−334.
(63) Lee, H.; Kim, S. C.; Chen, S.-C.; Segets, D.; Pui, D. Y. H. Predicting collision efficiencies of colloidal nanoparticles in single spherical and fibrous collectors using an individual particle tracking method. *Sep. Purif. Technol.* **2019**, *222*, 202−213.
(64) Elimelech, M.; Nagai, M.; Ko, C.-H.; Ryan, J. N. Relative insignificance of mineral grain zeta potential to colloid transport in geochemically heterogenous porous media. *Environ. Sci. Technol.* **2000**, *34*, 2143−2148.
(65) Goldberg, E.; Scheringer, M.; Bucheli, T. D.; Hungerbühler, K. Prediction of nanoparticle transport behavior from physicochemical properties: machine learning provides insights to guide the next generation of transport models. *Environ. Sci.: Nano* **2015**, *2*, 352−360.
(66) Babakhani, P.; Bridge, J.; Doong, R. a.; Phenrat, T. Parameterization and prediction of nanoparticle transport in porous media: A reanalysis using artificial neural network. *Water Resour. Res.* **2017**, *53*, 4564−4585.
(67) Zhou, K.; Li, S.; Zhou, X.; Hu, Y.; Zhang, C.; Liu, J. Data-driven prediction and analysis method for nanoparticle transport behavior in porous media. *Measurement* **2021**, *172*, 108869.
(68) Camesano, T. A.; Unice, K. M.; Logan, B. E. Blocking and ripening of colloids in porous media and their implications for bacterial transport. *Colloids Surf., A* **1999**, *160*, 291−307.
(69) Nascimento, A. G.; Tótola, M. R.; Souza, C. S.; Borges, M. T.; Borges, A. C. Temporal and spatial dynamics of blocking and ripening effects on bacterial transport through a porous media: A possible explanation for CFT deviation. *Colloids Surf., B* **2006**, *53*, 241−244.
(70) Li, J.; Zhang, W.; Qin, Y.; Li, X.; Wu, S.; Chai, J.; Du, S. Co-transport behavior of ammonium and colloids in saturated porous media under different hydrochemical conditions. *Environ. Sci. Pollut. Res.* **2020**, *27*, 15068−15082.
(71) Adamczyk, Z.; Siwek, B.; Zembala, M.; Weronski, P. Kinetics of localized adsorption of colloid particles. *Langmuir* **1992**, *8*, 2605−2610.
(72) Ko, C.-H.; Elimelech, M. The "shadow effect" in colloid transport and deposition dynamics in granular porous media: Measurements and mechanism. *Environ. Sci. Technol.* **2000**, *34*, 3681−3689.
(73) Torkzaban, S.; Tazehkand, S. S.; Walker, S. L.; Bradford, S. A. Transport and fate of bacteria in porous media: Coupled effects of chemical conditions and pore space geometry. *Water Resour. Res.* **2008**, *44*, W04403.
(74) Tong, M.; Ma, H.; Johnson, W. P. Funneling of flow into grain-to-grain contacts drives colloid-colloid aggregation in the presence of an energy barrier. *Environ. Sci. Technol.* **2008**, *42*, 2826−2832.
(75) Leoutsakos, G.; Crane, R. I. Three-dimensional boundary layer transition on a concave surface. *Int. J. Heat Fluid Flow* **1990**, *11*, 2−9.
(76) Winoto, S. H.; Tandiono; Shah, D. A.; Mitsudharmadi, H. On the development of concave surface boundary layer flows. *AIP Conf. Proc.* **2010**, *1225*, 10.
(77) Kemps, J. A. L.; Bhattacharjee, S. Particle tracking model for colloid transport near planar surfaces covered with spherical asperities. *Langmuir* **2009**, *25*, 6887−6897.
(78) Pazmino, E.; Trauscht, J.; Johnson, W. P. Release of colloids from primary minimum contact under unfavorable conditions by perturbations in ionic strength and flow rate. *Environ. Sci. Technol.* **2014**, *48*, 9227−9235.

https://doi.org/10.1021/acs.est.1c07305
Environ. Sci. Technol. 2022, 56, 4121−4131